2D and 3D Modeling of Electro-optic Effect in Whispering Gallery Mode Optical Microresonators

N. G. Pavlov[1,3], **N. M. Kondratyev**[1], **and M. L. Gorodetsky**[1,2]

[1]Russian Quantum Center, Russia
[2]Moscow State University, Russia
[3]Moscow Institution of Physics and Technology, Russia

Abstract— We present an analysis of electro-optic interaction of a fundamental WGM in a dielectric microdisc with a radio frequency mode of a half-wave microstrip resonator placed on the disc circumference. 2D and 3D numerical models of the system are developed. Both optical and radio frequency modes are simulated using finite element method with Comsol Multiphysics software. The comparison between the models is presented, and a theory of modulation in the multi-mode system is discussed. The magnitude of electro-optic effect is calculated depending on optical and radio frequency mode numbers and the microstrip length. The magnitude of the effect in such system is shown to have an extremal dependence on the microstrip length for a given set of mode numbers.

1. INTRODUCTION

Microwave systems, cellular networks and other various personal communications systems require devices that are capable of receiving, converting and processing signals in the millimeter and centimeter wave ranges. A broad palette of devices was developed recently for transferring radio frequency and microwave signals directly to optics [1]. This presents all advantages of optical communication channels, allowing to transmit data securely with high rates, low loss, low power consumption. Electro-optic modulators based on interaction of optical and microwave waves in high-Q nonlinear optical resonators with whispering gallery modes provide a promising platform of that kind [2–4].

Resonators with whispering gallery modes are widely used in various applications [5]. Small size and high density of the optical field in microcavities allows strong electro-optic interaction in resonators made of traditional nonlinear optical crystals, with proper selection of the optical modes and configuration of external high-frequency field.

2. THEORY OF WGM MODULATOR

The modulator consists of a semi-circular microstrip $\lambda/4$ resonator formed on top of an optical microdisk near it's circumference [3]. The microdisk plays the role of a dielectric layer for the microstrip, thus carrying the radio-frequency field. A schematic view of the modulator is shown on Figure 1. The resonator is made from electro-optical material, so an external electric field will lead to a change in the refractive index and the shift of the resonance frequency. Using perturbation theory, similar to [6], we obtain a general formula describing the frequency shift of the optical modes:

$$\frac{\delta\omega}{\omega} = \frac{1}{2}\frac{\int D_i^{\mathrm{WGM}_p *} r_{ijk} E_k^{RF} D_j^{\mathrm{WGM}} dV}{\epsilon_0 W^{\mathrm{WGM}}}, \tag{1}$$

where $\delta\omega$ is the frequency shift of the optical mode (signal), ω — its original frequency, D_j^{WGM} — j-component of the signal mode optical displacement field, and $D_j^{\mathrm{WGM}_p *}$ — complex conjugate of the pump mode field, $W^{\mathrm{WGM}} = \int \epsilon_0^{-1} D_i^{\mathrm{WGM}*} \epsilon_{ij}^{-1} D_j^{\mathrm{WGM}}$ is the total energy of the signal mode, and r_{ijk} is electrooptical coefficient. The integration is made over the volume of the microdisk and summation over all indices is performed.

Frequency shift (1) can be simplified by using the properties of whispering gallery modes and cylindrical symmetry [7] to 2D integral:

$$\frac{\delta\omega}{\omega} = \frac{\int_S r_{lmn}^{\mathrm{cyl}} E_n^{RF} D_l^{\mathrm{WGM}_p *} D_m^{\mathrm{WGM}} r dr dz}{2\epsilon_0 W^{\mathrm{WGM}}}. \tag{2}$$

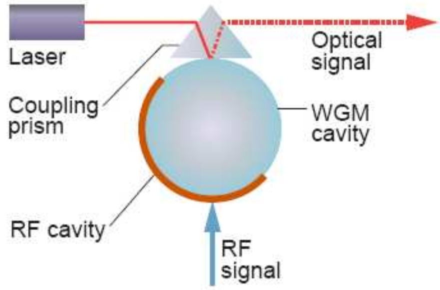

Figure 1: A scheme of the modulator.

In this derivation the $e^{i\frac{m_{rf}}{\alpha'}\varphi}$ azimuthal dependence is presumed for radio-frequency field, where α' is relative microstrip length (length divided by circle length). This assumption is discussed and verified further by modeling. Introducing a generalized azimuthal number $M = m_p - m_s + \frac{m_{rf}}{\alpha'}$ the r^{cyl}_{lmn} is given by

$$r^{cyl}_{lmn}(M,\alpha') = \sum_{k=-3}^{3} r^{cyl_k}_{lmn}\frac{\sin(\pi(M+k)\alpha')}{\pi(M+k)}e^{i\pi(M+k)\alpha'}. \tag{3}$$

The $r^{cyl_k}_{lmn}$ are dependent only on r_{ijk} ($r^{cyl_0}_{lmn}$ can be found in [7], taking $\epsilon_{ij} = 1$ there). The m_p, m_s and m_{rf} are azimuthal numbers ($\approx$ number of waves over the circumference) for the pumped mode, signal mode and radio-frequency mode. Note that for an open ring m_{rf} can be half integer due to the resonance condition of half-wave cavity.

The amplitude of the modulated signal is calculated starting from the Maxwell equations. Each mode is taken in the form of a slowly varying amplitude, oscillating with the pump frequency $u_j = A_j(t)e^{-i\omega t}$. Then

$$\left(\omega_k^2 - \omega^2\right)\frac{A_k}{c^2} + \frac{\ddot{A}_k}{c^2} - 2i\omega\frac{\dot{A}_k}{c^2} + \sum_j \frac{\partial^2}{\partial t^2}\frac{Uu_j}{c^2}2\delta_{\omega_{kj}} - \sum i\omega A_j\frac{2}{c^2}\kappa_{kj} = FX_k, \tag{4}$$

where, $\kappa_{kj} = \frac{c^2}{2}\gamma_j\frac{\int \vec{e}^{\dagger}_k\vec{e}_j dV}{\epsilon_0 W_k}$ — overlap integrals between neighboring modes, $X_k = \frac{\int \vec{e}^{\dagger}_k\vec{f}_p dV}{\epsilon_0 W_k}$ — overlap integral of the modes with the pump field, $\delta_{\omega_{kj}} = \frac{1}{2}\frac{\int \vec{e}^{\dagger}_k\hat{\epsilon}_1\vec{e}_j dV}{\epsilon_0 W_k}$ is a static frequency shift of the mode (1). U is a time dependence of modulation.

For a closed ring the modulation can be represented in two forms — a standing wave and traveling wave. In case of travelling wave the azimuthal and time dependencies are in the same cosine argument $U\hat{\epsilon}_1 \propto \cos(m_{RF}\varphi - \omega_{rf}t)$. Expanding the cosine into two exponents, we can introduce $\delta^+_{\omega_{kj}}$ and $\delta^-_{\omega_{kj}}$, which are calculated by (1), (2), (3) with $m_{RF} = +m_{RF}$ and $m_{RF} = -m_{RF}$ correspondingly. Assuming the derivative A and U with coefficients overlap $\delta_{\omega_{kj}}$ first order of smallness we obtain

$$\dot{A}_k = \sum_j \left(-i\Delta_k\delta_{kj} + i\left(\delta^-_{\omega_{kj}}\mu_+ e^{i\omega_{RF}t} + \delta^+_{\omega_{kj}}\mu_- e^{-i\omega_{RF}t}\right) - \kappa_{kj}\right)A_j + i\frac{Fc^2}{2\omega}X_k, \tag{5}$$

where $\Delta_k = \frac{\omega_k^2-\omega^2}{2\omega} \approx \omega_k - \omega$ and $\mu_\pm = \frac{(\omega\mp\omega_{RF})^2}{2\omega}$.

In case of an open ring we have only a standing wave case and time and space cosines are separate $\hat{\epsilon}_1 \propto \cos(m_{RF}\varphi)\cos(\omega_{RF}t)$. It is easy to see that the coefficients before the time exponentials in (5) are equal then, as if $\delta^+_{\omega_{kj}} = \delta^-_{\omega_{kj}} = \frac{\delta^+_{\omega_{kj}}+\delta^-_{\omega_{kj}}}{2}$.

We search for the solution in the form $b_k + a^-_k e^{-i\omega_{rf}t} + a^+_k e^{i\omega_{rf}t}$ with constant a and b. Neglecting the rapidly oscillating terms we obtain

$$a^\pm_k = \mu_\pm M^{-1}_\pm \delta^\mp_{\omega_{kj}} b_j, \tag{6}$$

$$b_k = \frac{Fc^2}{2\omega}B^{-1}X_k, \tag{7}$$

$M = \Delta_k \pm \omega_{RF} - e(\omega_{RF})\mu_\pm \delta^{\mp}_{\omega_{kj}} - i\kappa_{kj}$ and $\Delta_k - \mu_+\mu_-(\delta^{-}_{\omega_{km}} M_-^{-1} \delta^{+}_{\omega_{nj}} + \delta^{+}_{\omega_{km}} M_+^{-1} \delta^{-}_{\omega_{nj}}) - i\kappa_{kj}$. Here $\mathrm{e}(\omega_{RF})$ is an unknown function that is close to 1 for small ω_{RF} and close to 0 for high ω_{RF}. For the field amplitudes we obtain

$$b_k \approx \frac{Fc^2}{2\omega} \frac{X_k}{\Delta_k - i\kappa_{kk}} \left(1 - \sum_{j \neq k} \frac{X_j}{X_k} \frac{\kappa_{kj}}{\Delta_j - i\kappa_{jj}} \right), \tag{8}$$

$$a_k^{\pm} \approx \frac{(\omega \mp \omega_{RF})^2}{2\omega} \frac{\delta^{\mp}_{\omega_{kj}} b_j}{\Delta_k \pm \omega_{RF} - i\kappa_{kk}} \left(1 - \sum_{l \neq k} \frac{\delta^{\mp}_{\omega_{lj}} b_j}{\delta^{\mp}_{\omega_{kj}} b_j} \frac{\kappa_{kl}}{\Delta_l \pm \omega_{RF} - i\kappa_{ll}} \right). \tag{9}$$

As a result, each mode oscillates with the frequency of the pump with a constant amplitude b_k, proportional to the direct overlap with the mode pump X_k. Modulated part consists of oscillations at frequencies shifted relative to the pump at $\pm\omega_{rf}$, with amplitudes $a_k^{\pm}$, proportional to $\delta_{\omega_{kp}}$, i.e., the static efficiency shift of the mode. The traveling and standing wave modulation cases differ only in whether the δ_ω is the expression with azimuthal number of corresponding sign or their half-sum.

3. MICROWAVE MODES

For optimal performance of the modulator, the frequency matching due to (9) need to be satisfied: $f_{rf} = \Delta f^{opt}_{\mathrm{FSR}}$. The $\Delta f^{opt}_{\mathrm{FSR}} = \frac{c}{2\pi Rn}$ is the free spectral range of microdisk. Microwave frequency should be an integer multiple of free spectral range of the resonator.

Both optical and radio frequency modes were simulated using finite element method with Comsol Multiphysics software. Eigenfrequencies and distributions of the resonance fields in microstrip were calculated by two different methods.

The first method was the eigenvalue problem numerical solution in three-dimensional geometry. In the simulation, we changed the length of the strip in the range of $\alpha = \alpha' \times 360° \in [90°; 350°]$ and solved eigenvalue problem for each configuration separately. The result of numerical simulation for the length of the microstrip 160° is shown in Figure 2(a). This picture illustrates the distribution of the total electric field along the circumference of the WGM disc for half-wave mode of microstrip ($m_{rf} = 1/2$) with frequency $f_{rf} = 2.8$ GHz.

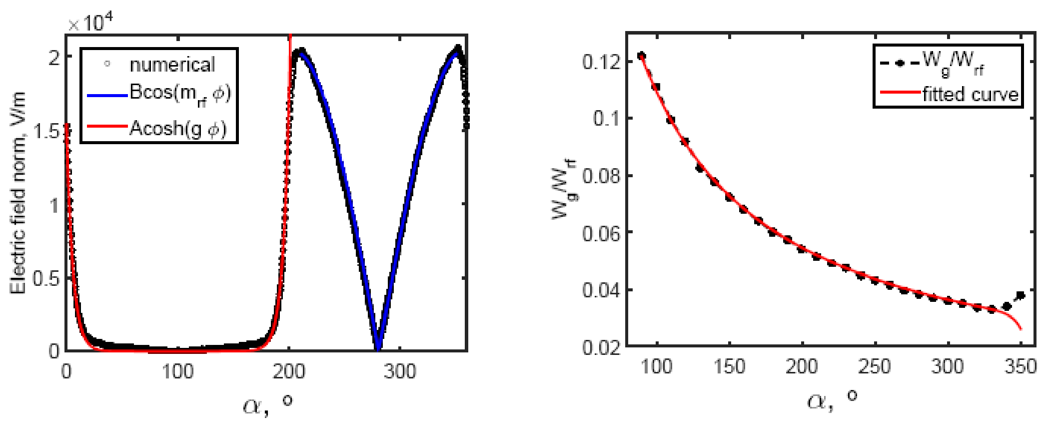

(a) (b)

Figure 2: (a) The distribution of the total electric field along the circumference of WGM microdisc for half-wave mode with of 160°-length ring. (b) The ratio of the evanescent field energy to the full microwave energy in the microstrip region for half-wave mode together with (10).

An evanescent field E_g can be seen at the ends of the microstrip, which decreases exponentially outside the microstrip region. The fitting curve $E_g = A\cosh(g\varphi)$ is drawn in red on a fig.2a. We also can see the clear cosine azimuthal dependence of the field inside the microstrip region in the same time. The $|\cos(\frac{m_{\mathrm{rf}}}{a}\varphi)|$ — blue curve on the graph.

Figure 2(b) shows the ratio $\frac{W_g}{W_{rf}}$ of the energy of the evanescent field to the microwave energy in the microstrip region. At angles $\alpha < 330°$ the evanescent field contributes up to 10% to the overall picture energy. That is because the exponential evanescent field (and thus its energy) is independent of the microstrip length, while the energy in the microstrip region decreases with α:

$$\frac{W_g}{W_{rf}} \propto \frac{2\int^{180^\circ-\alpha/2} e^{-2g\varphi} d\varphi}{\int^{\alpha} \cos\left(\frac{m_{rf}}{a}\varphi\right)^2 d\varphi} = \frac{1-e^{g(\alpha-360^\circ)}}{g\alpha}, \tag{10}$$

where g is the depth of the evanescent field propagation. For $\alpha > 330^\circ$ the evanescent fields from opposite ends interact and its energy grows.

In [7] the 2D geometry static problem (vertical section of the system, constant voltage on microstrip) was solved to represent the cross section field of the microstrip. To check that a corresponding problem in 3D case was solved in full geometry and then the ρ-z section was made. The comparison is made in the Figure 3.

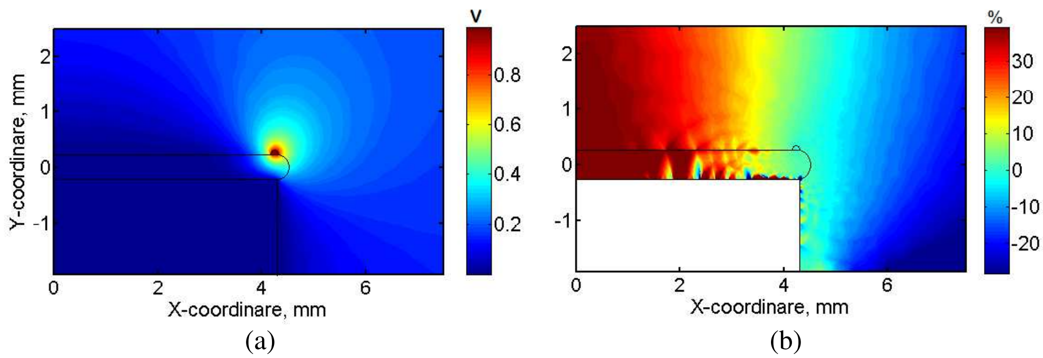

Figure 3: (a) Distribution of electric potential in the vertical section of the system, got from 3D model of static voltage. The microstrip section is clearly seen. (b) The difference between electric potentials in vertical section got from 2D model and 3D model in %. The white rectangle is the metal substrate under the WGM resonator.

It can be seen that the distributions are not actually equal and have differences at the boundaries of the modulator. This is due to the difficulty of boundary conditions specification in the numerical program. However, the difference at the edges is not important as the area of electro-optical interaction is under microstrip on the edge of microdisk, where the difference is about 1% accuracy. So the Figures 2 and 3 confirms the validity of approximations, used in [7] for Equation (2) derivation, that the microstrip field can be taken as $\vec{E}_{3D}(r,\phi,z) = \vec{E}_{2D}(r,z)\cos(\frac{m_{rf}}{a}\phi)$.

4. WGM MODES AND FREQUENCY SHIFT

To obtain the WGM field numerically, we use the method proposed in [8]. The method employs the solution of 2D eigenvalues problem in a cross section of cylindrically symmetric optical microcavity. WGMs are concentrated along the edges of the microdisc and its volume is small. Therefore it is necessary to concentrate the microwave field on the edge of the microdisc. It was also shown in [4], that the lower electrode has to be of the same diameter as the microresonator for the maximum overlap of microwave and optical fields.

Equation (1) describes the overlap integral in the form of dimensionless coefficient — relative frequency shift $\frac{\delta\omega}{\omega}$. However this shift differs for different applied modulating voltage. Furthermore the eigenvalue problem solution, which we use to find the fields, goes with arbitrary amplitude. That's why the quantity should be be normalized with the square root of the total electric energy $W^{RF} = \frac{1}{2}\int \epsilon_0 \epsilon^{RF} E_{RF} E^*_{RF} dV$. So we get the relative frequency shift per square root of joule.

Now we can calculate the frequency shifts in two different ways. First way is described in [7]: it performs analitycal integration over the azimuthal angle φ and numerical integration of 2D fields (2), obtained from static problem. In the second method we solve an eigenmode problem for the microstrip in 3D and then revolve the 2D WGM field to perform the numerical integration (1) in 3D.

The results are shown in Figure 4 for half-wave microstrip modes. The case of closed ring was not considered. The maximum shift is observed at ring lengths of 150°–280°.

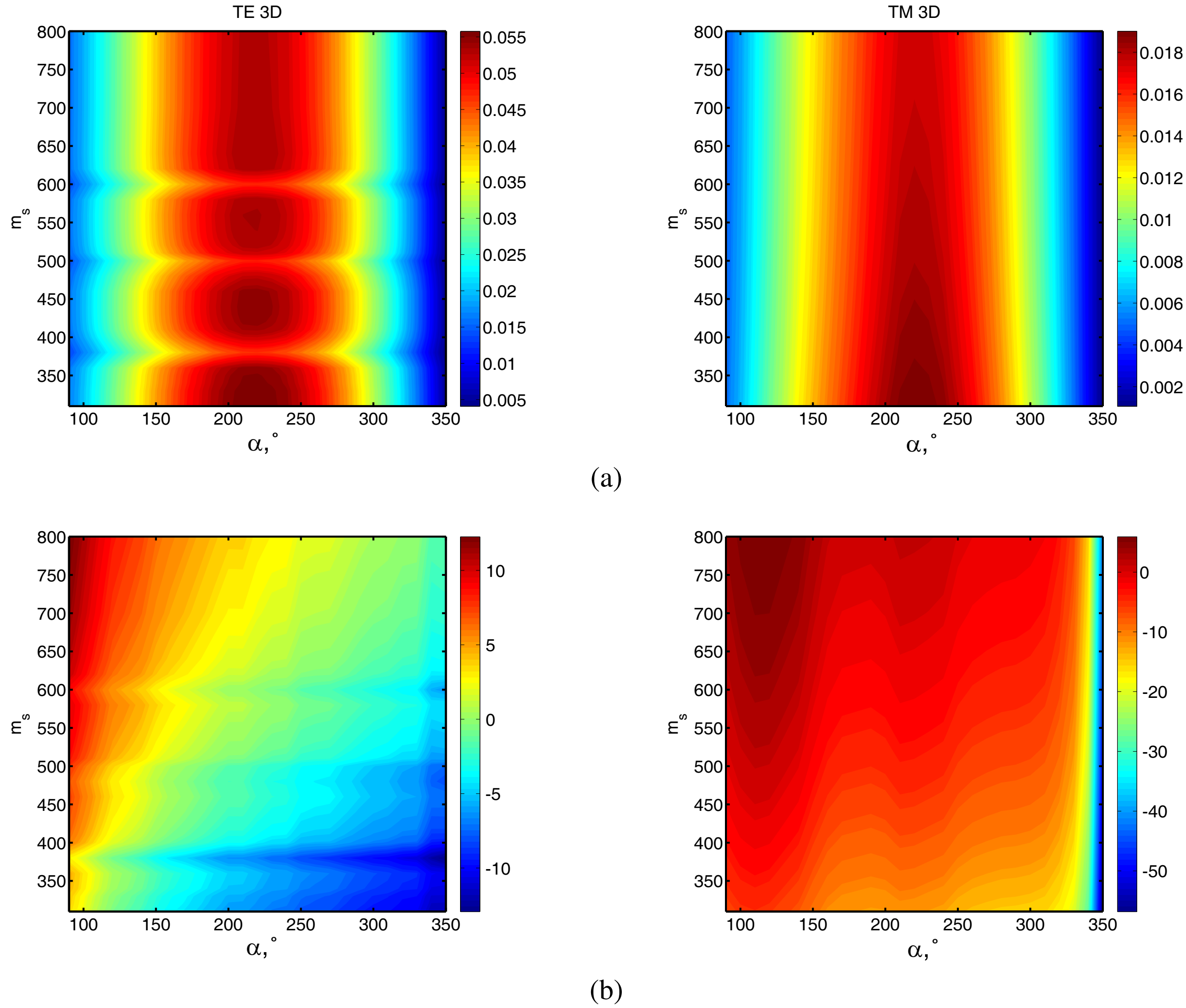

Figure 4: Frequency shifts per root of joule for TE and TM optical modes in (a) 3D model and their difference with (b) 2D model in %.

5. CONCLUSION

Though the 2D model works well for medium microstrip lengths and is much more efficient than the 3D model in terms of computational time, the latter is probably closer to reality. The difference is within 15% for TE optical modes, but over 50% for TMs. The main source of error is a evanescent field, which should be taken into account for short microstrips due to decrease of energy in it and for long microstrips due to interaction between it's ends.

The optimal microstrip length was found to be near 220°, where the efficiency is by 13% higher than for commonly used 180° length microstrips.

REFERENCES

1. Wooten, E. L., et al., "A review of lithium niobate modulators for fiber-optic communications systems," *IEEE Journal of Selected Topics in Quantum Electronics*, Vol. 1, No. 6, 69–82, 2000.
2. Hossein-Zadeh, M., "Photonic microwave receivers based on high-Q optical resonance," *Laser Resonators, Microresonators, and Beam Control XIV: Proceedings of SPIE*, Vol. 8236, 82360T1-10, San Francisco, CA, 2012.
3. Cohen, D. A., M. Hossein-Zadeh, and A. F. J. Levi, "Microphotonic modulator for microwave receiver," *Electronics Letters*, Vol. 37, 300–301, 2001.
4. Cohen, D. A., "Lithium niobate microphotonics modulators," PhD Thesis, Facility of the Graduate School, University of Southern California, 2001.
5. Ilchenko, V. S. and A. B. Matsko, "Optical resonators with whispering-gallery modes — Part II: Basics," *Selected Topics in Quantum Electronics*, Vol. 12, No. 1, 15–32, 2006.
6. Gorodetsky, M. L., *High-Q Optical Microresonators*, Fizmalit, Moscow, 2011.

7. Kondratiev, N. M. and M. L. Gorodetskiy, "Electrooptic interaction in whispering gallery mode resonators for radio frequency modulators," *Journal of Radio Electronics*, No. 11, 2012.
8. Oxborrow, M., "How to simulate the whispering-gallery-modes of dielectric microresonators in FemLab/Comsol," *Proc. SPIE 6452, Laser Resonators and Beam Control IX*, 64520J, 2007.